Quantum impurity in topological multi-Weyl semimetals

Hai-Feng Lü,[1,2,*] Ying-Hua Deng,[1] Sha-Sha Ke,[1,†] Yong Guo,[2] and Huai-Wu Zhang[1]

[1]*State Key Laboratory of Electronic Thin Films and Integrated Devices and Department of Applied Physics, University of Electronic Science and Technology of China, Chengdu 610054, China*

[2]*Department of Physics and State Key Laboratory of Low-Dimensional Quantum Physics, Tsinghua University, Beijing 100084, China*

(Received 22 October 2018; published 6 March 2019)

Multi-Weyl semimetals are new types of topological semimetals which have anisotropic nonlinear energy dispersion and whose topological charge can be 2 or more depending on the value of the winding number J. Here we investigate the Kondo effect of a spin-1/2 magnetic impurity in a multi-Weyl semimetal of different J by using the variational wave function method. For different J, the binding energy is always positive in the presence of broken inversion symmetry, and a bound state is favored to form between the impurity and the host electrons. It is found that the formed bound state is more stable for larger J. Due to the spin-orbit coupling, the components of spin-spin correlation functions $J_{uv}(\mathbf{r})$ $(u, v = x, y, z)$ show strong anisotropy in the coordinate space. The spin-spin correlation indicates distinct decay behaviors along different directions due to the anisotropic dispersion in the energy band. In the case of $J = 2$ and $J = 3$, the rotational symmetries of the spatial spin-spin correlations are displayed. Especially, the components J_{xx} and J_{yy} and J_{xy} and $-J_{yx}$ can be related through a $\pi/(2J)$ rotation.

DOI: 10.1103/PhysRevB.99.115109

I. INTRODUCTION

Topological semimetals are a new class of topological matter and have attracted increased attention because their energy bands host isolated crossing points protected by topology [1–24]. A Weyl semimetal is a kind of topological semimetal that supports Weyl fermions as low-energy excitations [1,5,12,13]. Due to the no-go theorem, Weyl fermions are always realized in pairs of opposite chirality and result when the degeneracy of a doubly degenerate Dirac point is lifted through broken inversion or time-reversal symmetry [25–29]. The topological charge of a Weyl node can be greater than 1 for winding numbers $J \geqslant 2$, and these materials are referred to as multi-Weyl semimetals. In contrast for the $J = 1$ class, the quasiparticle dispersion of the multi-Weyl semimetals $J \geqslant 2$ possesses a natural anisotropy, as displayed in Fig. 1. The double-Weyl nodes with $J = 2$ have been found in $HgCr_2Se_4$ [30,31] and $SrSi_2$ [32], and it has been predicted that $A(MoX)_3$ (with A=Rb, Tl; X=Te) [33] can accommodate Weyl points with $J = 3$. The charge-neutral Bogoliubov–de Gennes–Weyl quasiparticles with $J = 2$ have also been suggested to exist in superconducting states of ^{3}He-A [34], URu_2Si_2 [35], UPt_3 [36], SrPtAs [37], and YPtBi [38], for instance. Most previous theoretical and experimental studies focused on the properties of the simple Weyl systems ($J = 1$), possessing pairs of (anti)monopoles with unit charge. The classes with $J \geqslant 2$ remain much less explored [1,30,39–45]. It is thus highly desired to develop theoretical efforts to disclose the topological nature of the multi-Weyl semimetals.

The Kondo effect, which describes the low-temperature property of a quantum magnetic impurity or an Anderson impurity hosted in an electronic system [46], has been a long-standing issue for decades in condensed-matter physics. In a superconductor system, the detection of the impurity-induced states can be used to probe the pairing symmetry of the hosting superconductors [47]. For topological materials, it was found that the spin-orbit coupling between the impurity and the conduction electrons could lead to the anisotropic spin-spin correlation in both spin and spatial spaces [48,49]. With the rapid advance in exploring two-dimensional materials and topological materials, the impurity property has been widely investigated recently in various Dirac electronic systems, such as graphene [50,51], silicene [52], MoS_2 [53], the Dirac/Weyl semimetal [54,55], and tilted Dirac surface states [56].

The wave function of the Kondo singlet state can be described as a hybridization cloud centered at the impurity and decaying in the distance with a characteristic range R_K. When more than one impurity interacts with the conduction electrons, an effective Ruderman-Kittel-Kasuya-Yosida (RKKY) coupling between spatially localized magnetic moments arises, which oscillates with the distance between the impurities R and decays algebraically [57]. If the Kondo screening length R_K is shorter than the separation R, the antiferromagnetic Kondo coupling will be more important, and the RKKY interaction will not be observed. In the opposite case, the RKKY interaction will dominate. The RKKY-Kondo interplay has attracted much attention starting several decades ago and remains a hot topic of research because of its importance for new systems [58]. The RKKY interaction between magnetic impurities in single- and multi-Weyl semimetals has been widely studied in recent years [44,59–61].

Due to the anisotropic energy dispersion and abundant topological charges of a Weyl node, the electronic states near the Weyl points in multi-Weyl semimetals are expected

*lvhf04@uestc.edu.cn
†keshasha@uestc.edu.cn

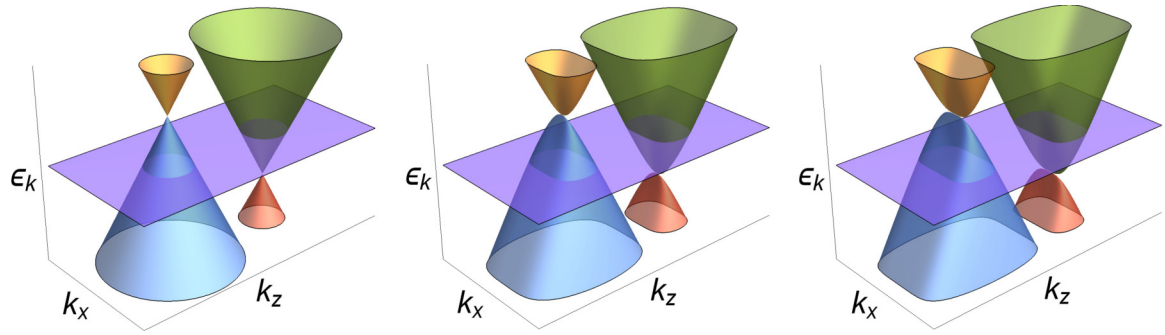

(a) $J = 1$ (b) $J = 2$ (c) $J = 3$

FIG. 1. The energy dispersion relationship of a multi-Weyl semimetal with (a) $J = 1$, (b) $J = 2$, and (c) $J = 3$ at $k_y = 0$. Both time-reversal and inversion symmetries are broken. Two nodal points are not at the same energy level.

to show a distinctive property. Motivated by these observations, here we systematically study the Kondo screening of a magnetic impurity in the multi-Weyl semimetals. The variational method is adopted to discuss the binding energy and the spin-spin correlations between the impurity and the conduction electrons. The quantum impurity in Weyl semimetals with $J = 1$ has been extensively investigated [55]. We generalize these studies to the cases of $J = 2$ and 3. We discuss the condition of forming a stable bound state for different J for comparison. The rotation symmetry and anisotropy in the spatial distribution of spin-spin correlations are also investigated.

This paper is organized as follows. In Sec. II, the model Hamiltonian is introduced, which describes a magnetic impurity in a multi-Weyl semimetal. In Sec. III, the variational method is introduced to discuss the binding energies of different winding numbers J and chemical potentials. In Sec. IV, we investigate the spin-spin correlation between the magnetic impurity and the conduction electrons in the multi-Weyl semimetal with different J. Finally, a summary is given in Sec. V.

II. ANDERSON MODEL HAMILTONIAN

We consider a spin-1/2 magnetic impurity in a three-dimensional multi-Weyl semimetal; the total Hamiltonian can be written as

$$\hat{H} = \hat{H}_0 + \hat{H}_d + \hat{H}_V, \tag{1}$$

where $\hat{H}_0$ is the free Hamiltonian operator of the multi-Weyl semimetal, $\hat{H}_d$ represents the Hamiltonian operator of the magnetic impurity, and $\hat{H}_V$ describes the hybridization between them. The minimal continuum Hamiltonian matrix for an isolated Weyl node of chirality s with both time-reversal and inversion symmetries broken is given by [45,62]

$$H_{\mathbf{k}s} = s[v_\perp k_0(\tilde{k}_-^J\sigma_+ + \tilde{k}_+^J\sigma_-) + v_z(k_z - sQ)\sigma_z - Q_0], \tag{2}$$

where $s = \pm 1$ stands for Weyl nodes of opposite chirality and J is the winding number. The velocity $v_\perp$ is the effective velocity of the quasiparticles in the plane perpendicular to the z axis, while v_z is the velocity along it. Here k_0 is a system-dependent parameter with the dimension of momentum. The broken time-reversal symmetry displaces the Weyl cone in momentum space by the amount $\pm Q$, and the broken inversion symmetry shifts the energy of Weyl nodes by $\pm Q_0$. We define the dimensionless parameters $\tilde{k}_\pm = k_\pm/k_0$, with $k_\pm = k_x \pm ik_y$ and $\sigma_\pm = \frac{1}{2}(\sigma_x \pm i\sigma_y)$, where $\sigma_i (i = x, y, z)$ is the Pauli matrix. Correspondingly, the free Hamiltonian of the multi-Weyl semimetal is given by

$$\hat{H}_0 = \sum_{\mathbf{k}s} \psi_{\mathbf{k}s}^\dagger H_{\mathbf{k}s}\psi_{\mathbf{k}s} - \mu, \tag{3}$$

where $\psi_{\mathbf{k}s}^\dagger = (c_{\mathbf{k}s\uparrow}^\dagger, c_{\mathbf{k}s\downarrow}^\dagger)$ and μ is the chemical potential of the system.

The local magnetic impurity Hamiltonian is

$$\hat{H}_d = (\varepsilon_d - \mu)(d_\uparrow^\dagger d_\uparrow + d_\downarrow^\dagger d_\downarrow) + U n_{d\uparrow} n_{d\downarrow}, \tag{4}$$

where $d_{\uparrow(\downarrow)}^\dagger$ and $d_{\uparrow(\downarrow)}$ are the creation and annihilation operators of the spin-up (spin-down) state on the impurity site and $n_{d\sigma} = d_\sigma^\dagger d_\sigma$. Here ε_d and U are the impurity energy level and on-site Coulomb repulsion, respectively. The hybridization between the magnetic impurity and the host material is described by

$$\hat{H}_V = \sum_{\mathbf{k}s\sigma} V_{\mathbf{k}}(d_\sigma^\dagger c_{\mathbf{k}s\sigma} + \text{H.c.}), \tag{5}$$

where $V_{\mathbf{k}}$ is the hybridization strength. Here we assume that the magnetic impurity is symmetrically coupled to the four bands in the semimetal for simplicity.

By diagonalizing the free Hamiltonian H_0, the single-particle eigenenergy $\varepsilon_{\mathbf{k}st}$ of the multi-Weyl semimetal is given by

$$\varepsilon_{\mathbf{k}st} = stv_\perp \sqrt{\frac{\left(k_x^2 + k_y^2\right)^J}{k_0^{2J-2}} + \frac{v_z^2}{v_\perp^2}(k_z - sQ)^2} - sQ_0 - \mu, \tag{6}$$

where $t = \pm$ stand for conduction (+) and valence (−) bands in the multi-Weyl semimetal. The energy spectrum $\varepsilon_{\mathbf{k}st}$ indicates a linear dependence on k_z and is proportional to the Jth power of $k_{x(y)}$ near the Fermi energy. The anisotropy of the dispersion relationship is expected to generate observable effects in the presence of the magnetic impurity.

The corresponding eigenstates operators of $\varepsilon_{\mathbf{k}st}$ are given by

$$\gamma_{\mathbf{k}st} = \sum_{\sigma} M_{\mathbf{k}st\sigma} c_{\mathbf{k}s\sigma}, \tag{7}$$

where the unitary matrix elements $M_{\mathbf{k}st\sigma}$ are

$$\begin{aligned} M_{\mathbf{k}st\uparrow} &= \frac{1}{\sqrt{2}} e^{iJ\theta_{\mathbf{k}}} \sqrt{1 + \frac{v_z(k_z - sQ)}{s(\varepsilon_{\mathbf{k}st} + \mu)}}, \\ M_{\mathbf{k}st\downarrow} &= \frac{1}{\sqrt{2}} \sqrt{1 - \frac{v_z(k_z - sQ)}{s(\varepsilon_{\mathbf{k}st} + \mu)}}, \end{aligned} \tag{8}$$

with $\theta_{\mathbf{k}} = \arctan(k_y/k_x)$.

We can rewrite the total Hamiltonian H in the diagonal basis as

$$\begin{aligned} \hat{H} = &\sum_{\mathbf{k}st} \varepsilon_{\mathbf{k}st} \gamma^{\dagger}_{\mathbf{k}st} \gamma_{\mathbf{k}st} + \sum_{\mathbf{k}st} V_{\mathbf{k}} (\gamma^{\dagger}_{\mathbf{k}st} d_{\mathbf{k}st} + \text{H.c.}) \\ &+ (\varepsilon_d - \mu) \sum_{\sigma} d^{\dagger}_{\sigma} d_{\sigma} + U\, d^{\dagger}_{\uparrow} d_{\uparrow} d^{\dagger}_{\downarrow} d_{\downarrow}, \end{aligned} \tag{9}$$

where the impurity operators $d_{\mathbf{k}st}$ are given by

$$d_{\mathbf{k}st} = \sum_{\sigma} M_{\mathbf{k}st\sigma} d_{\sigma}. \tag{10}$$

It is noted that the Hamiltonian of a multi-Weyl semimetal we adopt is based on the low-excitation approximation near the Weyl node. For a strong hybridization strength, the electrons far away from the Fermi surface make a greater contribution to the bound-state formation. In this case, the response of the impurity cannot reflect the electronic property near the Weyl points any more. Experimentally, the typical value of the hybridization V_k is on the order of 0.1–1 eV, which is generally weaker than the width of an energy band by one to two orders. For instance, V_k is about 0.25 eV for Co atoms on the Au (111) surface [63] and 0.5 eV in Ce compounds [64]. The energy range in which each Weyl node is well defined is generally of the order of 1–10 eV. For instance, the band structure in the prototypical case of Na_3Bi indicates well-defined Weyl nodes with an energy range of about 2 eV [65], while the Weyl nodes can be well defined with an energy range of more than 1 eV in NbP, TaP, and TaAs [66]. Therefore, our conclusion is applicable for most materials.

III. THE BINDING ENERGY

In the case of $V_{\mathbf{k}} = 0$, the hybridization between the impurity and the conduction electrons does not exist, and the ground state of H_0 is

$$|\Omega\rangle = \prod_{\{\mathbf{k}st\}} \gamma^{\dagger}_{\mathbf{k}st} |0\rangle, \tag{11}$$

where $\{\mathbf{k}st\}$ means the product (or sum) runs over all the states inside the Fermi surface (where $\varepsilon_{\mathbf{k}st} < 0$). If U is large enough and $\varepsilon_d < \mu < \varepsilon_d + U$, the impurity is singly occupied with a local moment. The total energy of the system is given by the sum of the energies of the host material and of the magnetic impurity,

$$E_0 = \varepsilon_d - \mu + \sum_{\{\mathbf{k}st\}} \varepsilon_{\mathbf{k}st}. \tag{12}$$

We then utilize the trial wave-function approach to investigate the property of the ground state of H in the presence of hybridization. For a large enough but finite Coulomb interaction U, ε_d is below the chemical potential, and the impurity site is always singly occupied. If the hybridization interaction is considered, the impurity state can be either unoccupied or singly occupied. Correspondingly, the trial ground state with hybridization can be written in the diagonal basis as

$$|\Psi\rangle = a_0 \left(1 + \sum_{\mathbf{k}st} a_{\mathbf{k}st} d^{\dagger}_{\mathbf{k}st} \gamma_{\mathbf{k}st}\right) |\Omega\rangle, \tag{13}$$

where a_0 and $a_{\mathbf{k}st}$ are variational parameters to be determined by minimizing the ground-state energy $E = \langle\Psi|H|\Psi\rangle/\langle\Psi|\Psi\rangle$. The ground-state energy of the total Hamiltonian H in the trial state $|\Psi\rangle$ can be evaluated as

$$E = \frac{\sum_{\{\mathbf{k}st\}} \left[(E_0 - \varepsilon_{\mathbf{k}st}) a^2_{\mathbf{k}st} + 2V_{\mathbf{k}} a_{\mathbf{k}st} + \varepsilon_{\mathbf{k}st}\right]}{1 + \sum_{\{\mathbf{k}st\}} a^2_{\mathbf{k}st}}. \tag{14}$$

The variational principle requires

$$\partial E/\partial a_{\mathbf{k}st} = 0, \tag{15}$$

from which we obtain

$$a_{\mathbf{k}st} = \frac{V_{\mathbf{k}}}{E - E_0 + \varepsilon_{\mathbf{k}st}}. \tag{16}$$

Substituting $a_{\mathbf{k}st}$ into Eq. (14), one can get

$$\begin{aligned} E - \sum_{\{\mathbf{k}st\}} \varepsilon_{\mathbf{k}st} &= \sum_{\{\mathbf{k}st\}} \left[-(E - E_0 + \varepsilon_{\mathbf{k}st}) a^2_{\mathbf{k}st} + 2V_{\mathbf{k}} a_{\mathbf{k}st} \right] \\ &= \sum_{\{\mathbf{k}st\}} \frac{V^2_{\mathbf{k}}}{E - E_0 + \varepsilon_{\mathbf{k}st}}. \end{aligned} \tag{17}$$

Finally, using the relationship in Eq. (12), the self-consistent equation about the binding energy $\Delta_b \equiv E_0 - E$ is deduced as

$$(\varepsilon_d - \mu) - \Delta_b = \sum_{\{\mathbf{k}st\}} \frac{V^2_{\mathbf{k}}}{\varepsilon_{\mathbf{k}st} - \Delta_b}. \tag{18}$$

If the binding energy $\Delta_b > 0$, the energy of the hybridized state is lower than that of the bare state, which means that the hybridized state is stabler. The summation over momentum in Eq. (18) is then replaced by the integration $\sum_{\mathbf{k}} \to V \int \frac{d^3k}{(2\pi)^3}$, and we get

$$\varepsilon_d - \mu - \Delta_b = V \sum_{st} \int d^3k \frac{V^2_{\mathbf{k}}}{\varepsilon_{\mathbf{k}st} - \Delta_b}, \tag{19}$$

where V is the volume of the system. In the following discussion, the hybridization $V_{\mathbf{k}}$ is assumed to be independent of $\mathbf{k}$ and can be defined as $V_{\mathbf{k}} = V_0 \Theta(\Lambda - \varepsilon_{\mathbf{k}st})$, with $\Theta(x)$ being the unit step function and Λ being the energy cutoff. In the calculation, we assume Λ serves as a convenient energy unit and define the effective hybridization $\Gamma = V_k^2/\Lambda^2$. The binding energy Δ_b can be obtained by solving Eq. (19)

numerically for different J. The parameter $a_{\mathbf{k}st}$ in the wave function is thus obtained from Eq. (16). In addition, the self-consistent equation for the binding energy can be expressed in an analytical form in the cases of $J = 1$ and 2. For $J = 1$, the self-consistent equation about the binding energy is given by

$$\Gamma = \frac{4\Lambda(\Delta_b + \mu - \varepsilon_d)/3}{\Lambda^2 - 4\Lambda\mu - 2\Delta_b\Lambda + 2\left[(\Delta_b + \mu)^2 + Q_0^2\right]\ln\frac{\Delta_b+\Lambda}{\Delta_b}}. \tag{20}$$

In the limit of $\Delta_b \ll \mu \ll \Lambda$ and for $Q_0 = 0$, one can obtain

$$\Delta_b \approx \Lambda\exp\left[\frac{1 - 2\pi^2 v_z v_\perp^2(\varepsilon_d - \mu)/\left(V\Lambda^2 V_k^2\right)}{2\mu^2/\Lambda^2}\right], \tag{21}$$

which agrees well with the results from the mean-field theory for the s-d exchange model [Eq. (A12) in the Appendix]. Actually, for the general case, it has been checked that the binding energy Δ_b correctly reproduces the Kondo energy $k_B T_K$ as given by the s-d model [67], i.e., $\Delta_b = k_B T_K$.

The self-consistent equation becomes more complicated for the case of $J = 2$. For $\mu < -Q_0$, the Fermi surface is below two nodal points, and the self-consistent equation for $J = 2$ is deduced as

$$\Gamma = \frac{\Delta_b + \mu - \varepsilon_d}{\Lambda + (\Delta_b + \mu)\ln\frac{\Delta_b}{\Delta_b+\Lambda}}. \tag{22}$$

For $|\mu| < Q_0$, the Fermi surface is between two nodal points, and

$$\frac{\Delta_b + \mu - \varepsilon_d}{\Gamma} = \Lambda - \mu - Q_0 + (\Delta_b + \mu)\ln\frac{\Delta_b + Q_0 + \mu}{\Delta_b + \Lambda} + Q_0\ln\frac{\Delta_b + Q_0 + \mu}{\Delta_b}; \tag{23}$$

for $\mu > Q_0$,

$$\frac{\Delta_b + \mu - \varepsilon_d}{\Gamma} = \Lambda - 2\mu + (\Delta_b + \mu)\ln\frac{(\Delta_b + \mu)^2 - Q_0^2}{(\Delta_b + \Lambda)\Delta_b} + Q_0\ln\frac{\Delta_b + Q_0 + \mu}{\Delta_b - Q_0 + \mu}. \tag{24}$$

Considering a simpler case in which $Q_0 = 0$, the binding energy in the limit $\Delta_b \ll \Lambda$ can be simplified as

$$\Delta_b \approx \Lambda\exp\left[\frac{1 - 4\pi v_z v_\perp(\varepsilon_d - \mu)/\left(V\Lambda k_0 V_k^2\right)}{|\mu|/\Lambda}\right] \tag{25}$$

for $\mu < 0$ and

$$\Delta_b \approx \frac{\mu^2}{\Lambda}\exp\left[\frac{1 - 4\pi v_z v_\perp(\varepsilon_d - \mu)/\left(V\Lambda k_0 V_k^2\right)}{|\mu|/\Lambda}\right] \tag{26}$$

for $\mu > 0$. The results for $J = 2$ also agree well with the results for the s-d exchange model [Eq. (A13) in the Appendix]. The Kondo temperature in the case of $J = 2$ is similar to the results for a single-Weyl semimetal in the two-dimensional case [48,68]. The reason is that in both cases the density of states indicates a similar dependence on energy, i.e., $\rho(\varepsilon) \sim |\varepsilon|$. For the case of $J \geqslant 3$, the self-consistent equation for the binding energy becomes rather complex, and here we do not present its analytical form.

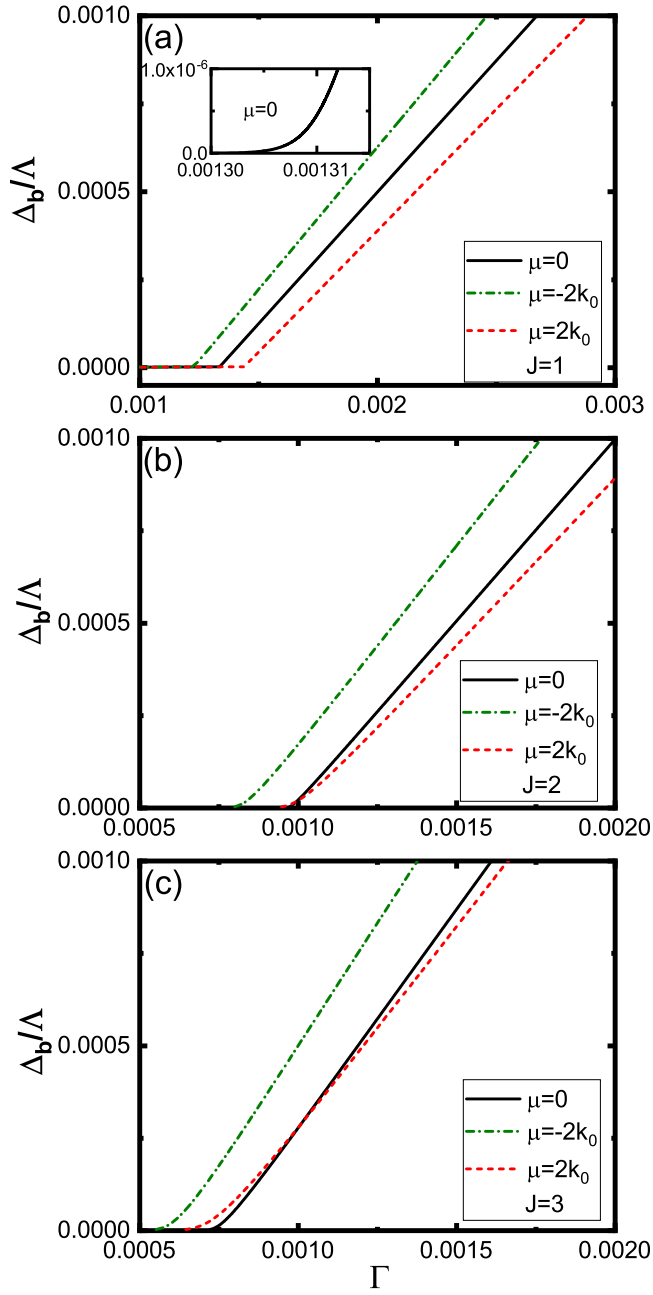

FIG. 2. Binding energy Δ_b of a magnetic impurity in a multi-Weyl semimetal with different J as a function of the hybridization. For the same binding energy, a larger J requires larger effective hybridization. The inset indicates that the binding energy is exponentially small with the decrease in Γ. The other parameters are taken to be $v_\perp k_0 = 10^{-2}\Lambda$, $v_z = 0.5 \times 10^{-2}\Lambda$, $Q = 2.5 \times 10^{-2}\Lambda$, $Q_0 = 0.5 \times 10^{-2}\Lambda$, and $\varepsilon_d - \mu = 0.1 \times 10^{-2}\Lambda$.

The binding energy is always positive for $\Gamma > 0$ and exponentially small with the decrease in Γ unless $\mu = Q_0 = 0$. Only in the case of $\mu = Q_0 = 0$ does a critical hybridization strength Γ_c to form a bound state exist. The magnetic impurity and the conduction electrons always favor forming a bound state in other cases. Such a result is also indicated in other Dirac materials [48,55,56,69]. Figure 2 demonstrates

the dependence of the binding energy Δ_b on the effective hybridization Γ for different winding numbers J and chemical potentials μ. In the calculation, we take $Q_0 \neq 0$, which implies that the inversion symmetry is broken. Correspondingly, the energies of two Weyl nodes are separated by $\pm Q_0$, and the position in the energy band is $(0, 0, \pm Q)$. We separately consider three different positions of the Fermi surface where it locates between, above, and below two nodal points, i.e., $\mu = 0, \pm 2 \times 10^{-2}\Lambda$. For weak hybridization Γ, the binding energy is exponentially small with the decrease in Γ. In this case, the formed bound state can easily be destroyed by small thermal fluctuations. The stable bound state exists only for a large binding energy. As shown in Fig. 2, the weaker hybridization Γ is required for the larger J to form a stable bound state.

It is clear that a k-dependent hybridization $V_{\mathbf{k}}$ can affect the binding energy value when solving the self-consistent equation (18). Actually, for orbits which couple with the continuum via V_k, which depends on the azimuthal angle, a similar result would ensue for $J = 1$. For example, for d_{xz} and d_{yz} we have $V_{\mathbf{k}} = V_k \cos\varphi$ and $V_{\mathbf{k}} = V_k \sin\varphi$, respectively. However, for $d_{x^2-y^2}$ and d_{xy}, we have $V_{\mathbf{k}} = V_k \cos 2\varphi$ and $V_{\mathbf{k}} = V_k \sin 2\varphi$, respectively. It is easy to see that only a mere shift is induced by the angular additional factors in the integral of Eq. (18). In this case, we can use the same effective model, but with different combinations of continuum states coupling to the impurity. In the case of $J = 2$ and 3, a k-dependent hybridization affects the results in a more complex way due to the stronger anisotropic dispersion relationship. Nevertheless, it can be checked that a k-dependent hybridization $V_{\mathbf{k}}$ does not change the results in a qualitative way.

In Fig. 2 we consider the case of broken time-reversal symmetry $Q \neq 0$. The Kondo effect and ferromagnetism are generally competing to influence the ground state of a single magnetic impurity. A strong enough magnetic field corresponding to a Zeeman energy above the binding energy of the Kondo singlet (about the Kondo temperature) will break up the singlet. In transport systems (such as quantum dot devices), the imbalance between spin-up and spin-down states in the host metal should cause the resonance to split into two asymmetric peaks. Experimentally, the Kondo effect in ferromagnetic Weyl semimetals could be detected by the use of scanning tunneling microscopy [70–72], in which a tip can approach and contact a single magnetic impurity on a surface. The splitting of the Kondo peak in the conductance characterizes the fingerprint of itinerant magnetism in the host.

IV. SPIN-SPIN CORRELATION

In this section, we study the spin-spin correlation between the magnetic impurity $S_d = \frac{1}{2} d^\dagger \sigma d$ at the impurity site and the conduction electron spin $S_c = \frac{1}{2} c^\dagger \sigma c$ of the ground state in a multi-Weyl semimetal. The spin-spin correlation function is evaluated for the positive binding energy $\Delta_b > 0$; that is, Kondo screening exists. We assume that the impurity is located at the origin $\mathbf{r} = 0$. The spin-spin correlation function is

$$J_{uv}(\mathbf{r}) = \langle \Psi | S_c^u(\mathbf{r}) S_d^v(0) | \Psi \rangle, \tag{27}$$

where $\mathbf{r}$ is the displacement between the impurity and conduction electrons, $u, v = x, y, z$, and $\langle \cdots \rangle$ denotes the ground-state average.

Because

$$\langle \Omega | \gamma^\dagger_{\mathbf{k}st} \gamma^\dagger_{\mathbf{q}zo} \gamma_{\mathbf{q}'z'o'} \gamma_{\mathbf{k}'s't'} | \Omega \rangle = \delta_{\mathbf{qq}'} \delta_{zz'} \delta_{\mathbf{kk}'} \delta_{ss'} \delta_{\mathbf{tt}'} \delta_{\mathbf{oo}'} - \delta_{\mathbf{kq}'} \delta_{sz'} \delta_{\mathbf{qk}'} \delta_{zs'} \delta_{\mathbf{to}'} \delta_{\mathbf{ot}'}, \tag{28}$$

it is obtained from Eqs. (7) and (10) that

$$\langle \Psi | d^\dagger_{\sigma_1} c^\dagger_{s\sigma_2}(\mathbf{r}) c_{s\sigma_3}(\mathbf{r}) d_{\sigma_4} | \Psi \rangle = C_0 - a_0^2 \sum_{\{\mathbf{k}_3 t_3\}} e^{i\mathbf{k}_3\cdot\mathbf{r}} a_{\mathbf{k}_3 s t_3} M_{\mathbf{k}_3 s t_3 \sigma_1} M^*_{\mathbf{k}_3 s t_3 \sigma_3} \times \sum_{\{\mathbf{k}_2 t_2\}} e^{-i\mathbf{k}_2\cdot\mathbf{r}} a_{\mathbf{k}_2 s t_2} M^*_{\mathbf{k}_2 s t_2 \sigma_4} M_{\mathbf{k}_2 s t_2 \sigma_2}, \tag{29}$$

where C_0 is a constant. Correspondingly, we can define functions below and combine them into the spin-spin correlation function $J_{uv}(\mathbf{r})$ in the coordinate space,

$$A_{s\sigma_1\sigma_3}(\mathbf{r}) = \frac{1}{2} a_0 \sum_{\{\mathbf{k}t\}} e^{i\mathbf{k}\cdot\mathbf{r}} a_{\mathbf{k}st} M_{\mathbf{k}st\sigma_1} M^*_{\mathbf{k}st\sigma_3}. \tag{30}$$

The diagonal terms of the spin-spin correlation function along the three axes are given by

$$\begin{aligned} J_{zz}(\mathbf{r}) &= \sum_s (-|A_{s\uparrow\uparrow}|^2 + |A_{s\uparrow\downarrow}|^2 + |A_{s\downarrow\uparrow}|^2 - |A_{s\downarrow\downarrow}|^2), \\ J_{xx}(\mathbf{r}) &= -2 \sum_s \mathrm{Re}\{A_{s\uparrow\downarrow} A^*_{s\downarrow\uparrow} + A_{s\uparrow\uparrow} A^*_{s\downarrow\downarrow}\}, \\ J_{yy}(\mathbf{r}) &= 2 \sum_s \mathrm{Re}\{A_{s\uparrow\downarrow} A^*_{s\downarrow\uparrow} - A_{s\uparrow\uparrow} A^*_{s\downarrow\downarrow}\}, \end{aligned} \tag{31}$$

and the nonzero off-diagonal parts are given by

$$\begin{aligned} J_{xy}(\mathbf{r}) &= -2 \sum_s \mathrm{Im}\{A_{s\uparrow\downarrow} A^*_{s\downarrow\uparrow} + A_{s\uparrow\uparrow} A^*_{s\downarrow\downarrow}\}, \\ J_{yx}(\mathbf{r}) &= 2 \sum_s \mathrm{Im}\{A_{s\uparrow\uparrow} A^*_{s\downarrow\downarrow} - A_{s\uparrow\downarrow} A^*_{s\downarrow\uparrow}\}, \\ J_{xz}(\mathbf{r}) &= 2 \sum_s \mathrm{Re}\{A_{s\downarrow\downarrow} A^*_{s\downarrow\uparrow} - A_{s\uparrow\downarrow} A^*_{s\uparrow\uparrow}\}, \\ J_{zx}(\mathbf{r}) &= 2 \sum_s \mathrm{Re}\{A_{s\uparrow\downarrow} A^*_{s\downarrow\downarrow} - A_{s\uparrow\uparrow} A^*_{s\downarrow\uparrow}\}, \\ J_{yz}(\mathbf{r}) &= 2 \sum_s \mathrm{Im}\{A_{s\downarrow\downarrow} A^*_{s\downarrow\uparrow} - A_{s\uparrow 2} A^*_{s\uparrow\uparrow}\}, \\ J_{zy}(\mathbf{r}) &= 2 \sum_s \mathrm{Im}\{A_{s\uparrow\downarrow} A^*_{s\downarrow\downarrow} - A_{s\uparrow\uparrow} A^*_{s\downarrow\uparrow}\}. \end{aligned} \tag{32}$$

In the case of $J = 2$, the spatial distributions of the spin-spin correlations for different μ along the x axis and the z axis are plotted in Figs. 3 and 4, respectively. For simplicity, we fix $V_0 = 3.8 \times 10^{-2}\Lambda$, and other parameters are the same as those in Fig. 2. Around the magnetic impurity, the diagonal components of spin-spin correlations at a short distance are negative, embodying an antiferromagnetic correlation between the impurity and the conduction electrons. For the

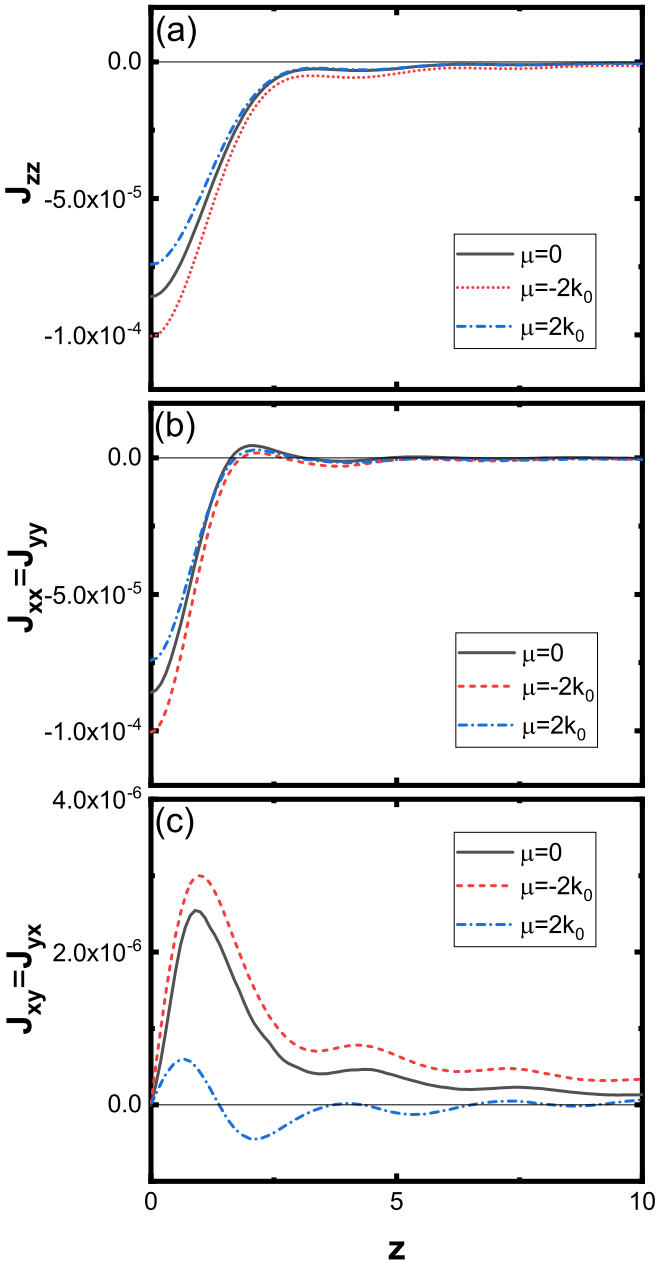

FIG. 3. Spatial spin-spin correlation functions (a) $J_{zz}(0,0,z)$, (b) $J_{xx}(0,0,z)$ [$=J_{yy}(0,0,z)$], and (c) $J_{xy}(0,0,z)$ [$=J_{yx}(0,0,z)$] as functions of z for $J=2$, $V_0=3.8\times10^{-2}\Lambda$, and other parameters as in Fig. 2. Other components of $J_{uv}(0,0,z)$ are zero. The length unit is $v_\perp/k_0$. $J_{xy}(0,0,z)$ [$=J_{yx}(0,0,z)$] is an odd function on the z axis.

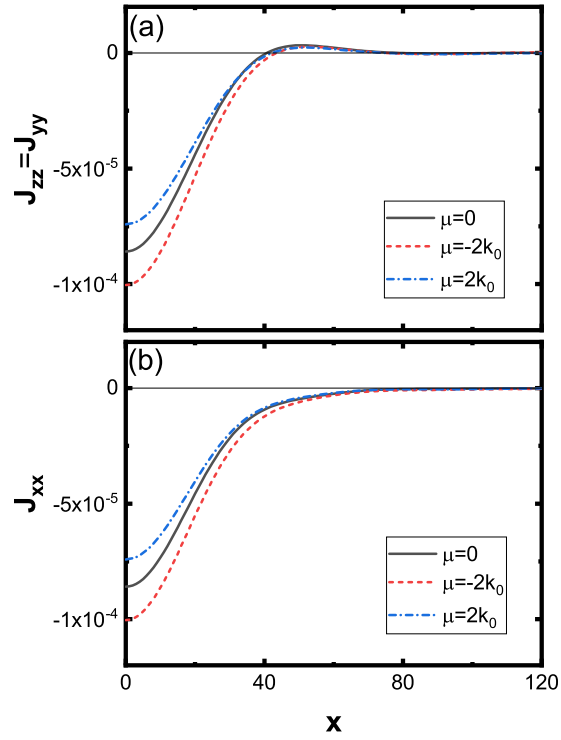

FIG. 4. Spatial spin-spin correlation functions (a) $J_{zz}(x,0,0)$ [$=J_{yy}(x,0,0)$], (b) $J_{xx}(x,0,0)$, (c) $J_{xy}(x,0,0)$ [$=J_{yx}(x,0,0)$] along the x axis with $J=2$. The off-diagonal components are zero. The diagonal components of spin-spin correlations with different μ show qualitatively similar features on the x axis.

spin-spin correlation component J_{xx} (J_{zz}) along the x (z) axis, the antiferromagnetic behavior around the magnetic impurity remains unchanged. The off-diagonal terms embody the effect of the spin-orbit coupling in the multi-Weyl semimetals. Figure 3(c) shows that $J_{xy}(\mathbf{r})$ and $J_{yx}(\mathbf{r})$ oscillate along the x axis and are much weaker than the diagonal components given in Figs. 3(a) and 3(b). The other off-diagonal terms of the spin-spin correlation are exactly zero.

To investigate the effect of the winding number on the impurity property, the spatial distributions of the spin-spin correlations along the x axis for different winding numbers $J=1,2$, and 3 are illustrated in Fig. 5. For comparison, we take the chemical potential $\mu=-2\times10^{-2}\Lambda$ and fix the binding energy $\Delta_b=0.038\times10^{-2}\Lambda$. The spin-spin correlations for $J=1$ decay faster along the x axis than the case of $J=2$ and 3. This J-dependent decay behavior of the spin-spin correlations originates from the anisotropic energy dispersion relationship. As shown in Fig. 1, the symmetry between the k_x and k_z axes in the energy dispersion for $J=1$ is broken for the higher-winding-number case ($J>1$). The broken symmetry in the momentum space is reflected in the spin-spin correlation in real space. Figures 3 and 4 demonstrate that, for $J=2$, all the components of spin-spin correlation decay faster along the z axis and slower along the x axis. This anisotropy of the decay behavior of spin-spin correlation functions can also be observed for $J=3$, while it does not appear for $J=1$ [55]. The anisotropic decay is induced by the different dispersion relationships of the energy band in the $x(y)$ and z directions. Therefore, it is expected that the decay property of the spin-spin correlations can provide a fingerprint to discriminate the topological charge of the Weyl node.

The spin-spin correlations in the x-y plane for the cases of $J=2$ and $J=3$ are demonstrated in Figs. 6 to 9. We first discuss the case of $J=2$. Figures 6 and 7 indicate the spin-spin correlations for $J=2$, where the components not presented here are zero in the x-y plane. As we can see, the components $J_{xx}(x,y,0)$, $J_{yy}(x,y,0)$, $J_{xy}(x,y,0)$, and $J_{yx}(x,y,0)$ are anisotropic in this plane, while J_{zz} is rotation invariant and $J_{zz}(r,0,0)=J_{yy}(r,0,0)=J_{xx}(0,r,0)$. As $\theta_{\mathbf{k}}$ changes, the off-

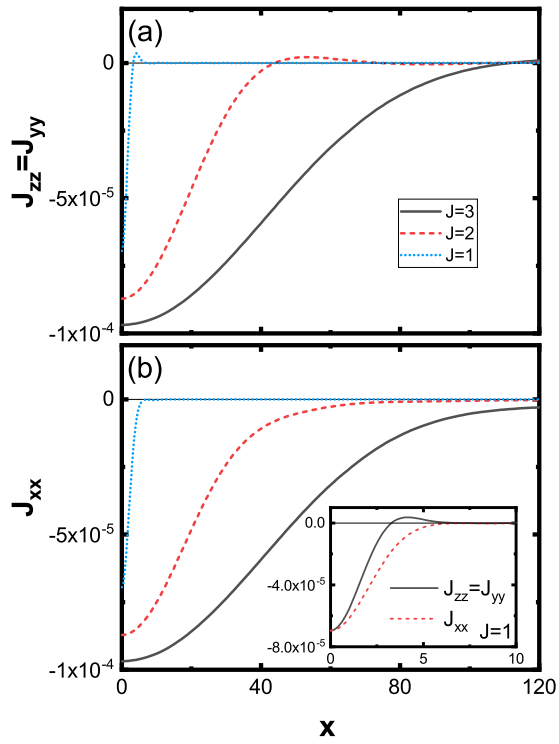

FIG. 5. Comparison between spin-spin correlation functions of $J = 1, 2, 3$ with $\Delta_b = 0.038 \times 10^{-2}\Lambda$ and $\mu = -2 \times 10^{-2}\Lambda$ on the x axis. For smaller J, the spin-spin correlations around the impurity decay faster.

off-diagonal components J_{xy} and J_{yx} oscillate between positive and negative values. In Fig. 7, we modulate the strength scale

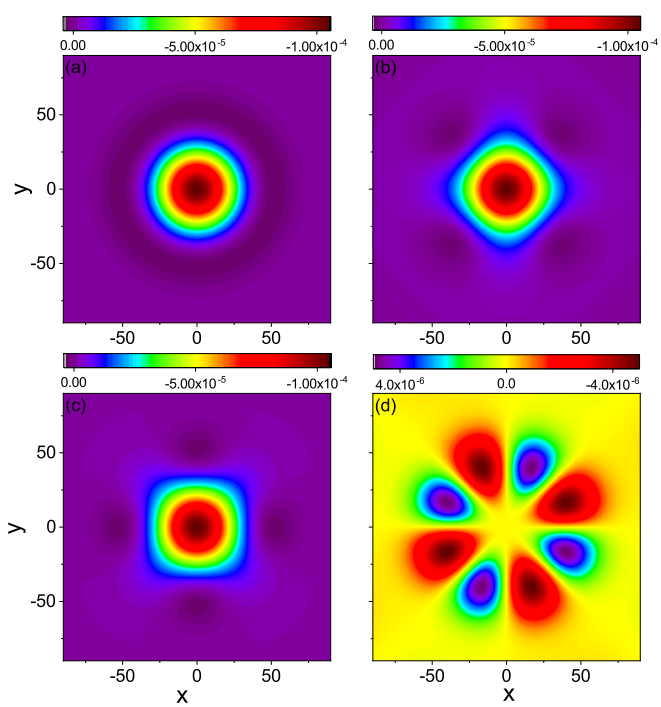

FIG. 6. Spatial spin-spin correlation functions with $J = 2$ plotted on the x-y plane. (a) $J_{zz}(x, y, 0)$, (b) $J_{xx}(x, y, 0)$, (c) $J_{yy}(x, y, 0)$, and (d) $J_{xy}(x, y, 0) = J_{yx}(x, y, 0)$. The parameters are set to $\mu = -2 \times 10^{-2}\Lambda$ and $V_0 = 3.8 \times 10^{-2}\Lambda$.

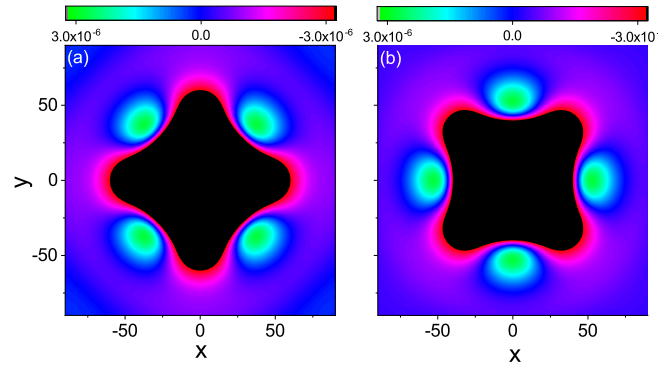

FIG. 7. To show the symmetrical characteristic of (a) $J_{xx}(x, y, 0)$ and (b) $J_{yy}(x, y, 0)$ more clearly, the strength scale is modulated. Apparently, $J_{xx}(x, y, 0)$ and $J_{yy}(x, y, 0)$ are related by a $\pi/4$ rotation.

of the spin-spin correlations J_{xx} and J_{yy} to illustrate their rotation symmetry more clearly. It is shown that $J_{xx}(x, y, 0)$ and $J_{yy}(x, y, 0)$ and $J_{xy}(x, y, 0)$ and $-J_{yx}(x, y, 0)$ are related to each other by a $\pi/4$ rotation. These four components are all $\mathbf{C}_4$ symmetric.

The spatial spin-spin correlation functions of $J = 3$ are displayed in Figs. 8 and 9. Similar to the case of $J = 2$, the diagonal components of spin-spin correlations are also antiferromagnetic at short distance. For $J = 3$, $J_{xx}(x, y, 0)$ and $J_{yy}(x, y, 0)$ and $J_{xy}(x, y, 0)$ and $-J_{yx}(x, y, 0)$ are related to each other by a $\pi/6$ rotation, and these four components are all $\mathbf{C}_6$ symmetric. Different from the case of $J = 2$, the components $J_{xz} = -J_{zx}$ and $J_{yz} = -J_{zy}$ of the spin-spin correlations are nonzero for $J = 3$, and they all have $\mathbf{C}_3$ symmetry. Therefore,

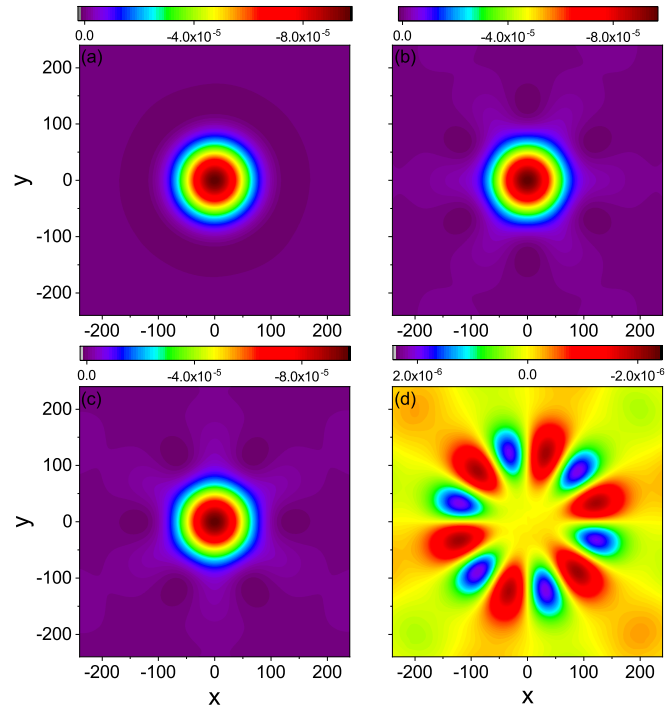

FIG. 8. Spatial spin-spin correlation functions with $J = 3$ plotted on the x-y plane. (a) $J_{zz}(x, y, 0)$, (b) $J_{xx}(x, y, 0)$, (c) $J_{yy}(x, y, 0)$, and (d) $J_{xy}(x, y, 0) = J_{yx}(x, y, 0)$. The parameters are set to $\mu = -2 \times 10^{-2}\Lambda$, $V_0 = 3.5 \times 10^{-2}\Lambda$.

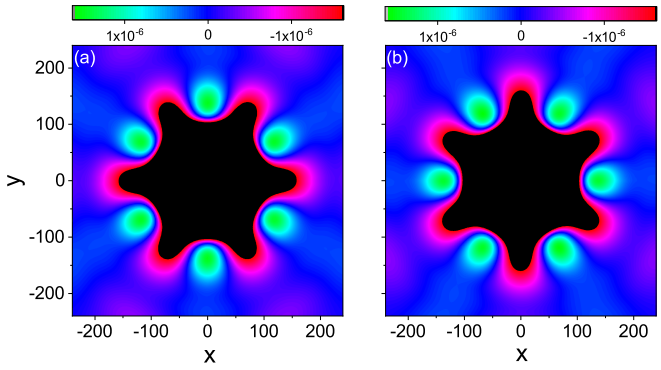

FIG. 9. To show the symmetrical characteristic of (a) $J_{xx}(x, y, 0)$ and (b) $J_{yy}(x, y, 0)$ more clearly, the strength scale is modulated. Apparently, $J_{xx}(x, y, 0)$ and $J_{yy}(x, y, 0)$ are related by a $\pi/6$ rotation.

we can see the topological charge J from the symmetry property of the spatial spin-spin correlations.

The $\mathbf{C}_J$ symmetry of the spatial distribution of spin-spin correlation functions in the x-y plane results from the form of the Hamiltonian. The Hamiltonian matrix $H_{\mathbf{k}s}$ satisfies

$$\begin{aligned} H_{\mathbf{k}s} &= \begin{pmatrix} v_z(k_z - sQ) - Q_0 & \frac{v_\perp}{k_0^{J-1}} e^{-iJ\theta_{\mathbf{k}}} k_\perp^J \\ \frac{v_\perp}{k_0^{J-1}} e^{iJ\theta_{\mathbf{k}}} k_\perp^J & -v_z(k_z - sQ) - Q_0 \end{pmatrix} \\ &= \begin{pmatrix} v_z(k_z - sQ) - Q_0 & \frac{v_\perp}{k_0^{J-1}} e^{-i(J\theta_{\mathbf{k}}+2\pi)} k_\perp^J \\ \frac{v_\perp}{k_0^{J-1}} e^{i(J\theta_{\mathbf{k}}+2\pi)} k_\perp^J & -v_z(k_z - sQ) - Q_0 \end{pmatrix} \\ &= \begin{pmatrix} v_z(k_z - sQ) - Q_0 & \frac{v_\perp}{k_0^{J-1}} e^{-iJ(\theta_{\mathbf{k}}+2\pi/J)} k_\perp^J \\ \frac{v_\perp}{k_0^{J-1}} e^{iJ(\theta_{\mathbf{k}}+2\pi/J)} k_\perp^J & -v_z(k_z - sQ) - Q_0 \end{pmatrix} \\ &= \begin{pmatrix} v_z(k_z - sQ) - Q_0 & \frac{v_\perp}{k_0^{J-1}} e^{-iJ\theta_{\mathbf{R}_J\mathbf{k}}} k_\perp^J \\ \frac{v_\perp}{k_0^{J-1}} e^{iJ\theta_{\mathbf{R}_J\mathbf{k}}} k_\perp^J & -v_z(k_z - sQ) - Q_0 \end{pmatrix} \\ &= H_{\mathbf{R}_J\mathbf{k}s}, \end{aligned} \tag{33}$$

and its eigenvalues meet the relationship $\varepsilon_{\mathbf{k}st} = \varepsilon_{\mathbf{R}_J\mathbf{k}st}$, where $\mathbf{R}_J$ is the rotation matrix for the $2\pi/J$ rotation in the x-y plane in the vector space and $k_\perp = k_x^2 + k_y^2$. Correspondingly, the unitary matrix $M_{\mathbf{k}st\sigma}$ in Eq. (7) has the property

$$M_{\mathbf{k}st\sigma} = M_{\mathbf{R}_J\mathbf{k}st\sigma}. \tag{34}$$

Noting $V_{\mathbf{k}} = V_{\mathbf{R}_J\mathbf{k}}$, the variational parameters $a_{\mathbf{k}st}$ meet

$$a_{\mathbf{k}st} = a_{\mathbf{R}_J\mathbf{k}st}, \tag{35}$$

so the functions $A_{s\sigma_1\sigma_3}(\mathbf{r})$ in Eq. (30) satisfy

$$\begin{aligned} A_{s\sigma_1\sigma_3}(\mathbf{r}) &= \frac{1}{2}\sum_{\{\mathbf{k}t\}} e^{-i\mathbf{k}\cdot\mathbf{r}} a_{\mathbf{k}st} M_{\mathbf{k}st\sigma_1} M^*_{\mathbf{k}st\sigma_3} \\ &= \frac{1}{2}\sum_{(\mathbf{R}_J\{\mathbf{k}\}t\}} e^{-i(\mathbf{R}_J\mathbf{k})\cdot(\mathbf{R}_J\mathbf{r})} a_{\mathbf{R}_J\mathbf{k}st} M_{\mathbf{R}_J\mathbf{k}st\sigma_1} M^*_{\mathbf{R}_J\mathbf{k}st\sigma_3} \\ &= A_{s\sigma_1\sigma_3}(\mathbf{R}_J\mathbf{r}), \end{aligned} \tag{36}$$

and the spin-spin correlations are $\mathbf{C}_J$ symmetric,

$$J_{uv}(\mathbf{r}) = J_{uv}(\mathbf{R}_J\mathbf{r}). \tag{37}$$

Performing the $\pi/(2J)$ rotation (denoted as $\mathbf{R}_{4J}$), it can be deduced from Eqs. (8) and (30)

$$\begin{aligned} A_{s\uparrow\downarrow}(\mathbf{R}_{4J}\mathbf{r}) &= \frac{1}{4}\sum_{\{\mathbf{k}t\}} e^{i\mathbf{k}\cdot\mathbf{R}_{4J}\mathbf{r}} a_{\mathbf{k}st} e^{iJ\theta_{\mathbf{k}}} \left(1 - \frac{v_z^2(k_z - sQ)^2}{(E_{\mathbf{k}st} + \mu)^2}\right)^2 \\ &= \frac{1}{4}\sum_{\{\mathbf{k}'t\}} e^{i\mathbf{k}'\cdot\mathbf{r}} a_{\mathbf{k}'st} e^{iJ\theta_{\mathbf{R}_{4J}\mathbf{k}'}} \left(1 - \frac{v_z^2(k_z - sQ)^2}{(E_{\mathbf{k}'st} + \mu)^2}\right)^2 \\ &= \frac{1}{4}\sum_{\{\mathbf{k}'t\}} e^{i\mathbf{k}'\cdot\mathbf{r}} a_{\mathbf{k}'st} e^{iJ\theta_{\mathbf{k}'}+i\pi/2} \left(1 - \frac{v_z^2(k_z - sQ)^2}{(E_{\mathbf{k}'st} + \mu)^2}\right)^2 \\ &= iA_{s\uparrow\downarrow}(\mathbf{r}), \end{aligned} \tag{38}$$

where $\mathbf{k}' = \mathbf{R}_{-4J}\mathbf{k}$. Similarly, one can find that

$$\begin{aligned} &A_{s\uparrow\uparrow}(\mathbf{R}_{4J}\mathbf{r}) = A_{s\uparrow\uparrow}(\mathbf{r}), \quad A_{s\downarrow\downarrow}(\mathbf{R}_{4J}\mathbf{r}) = A_{s\downarrow\downarrow}(\mathbf{r}), \\ &A_{s\downarrow\uparrow}(\mathbf{R}_{4J}\mathbf{r}) = -iA_{s\downarrow\uparrow}(\mathbf{r}). \end{aligned} \tag{39}$$

Substituting these relationships into Eqs. (31) and (32), it can be proved that

$$\begin{aligned} &J_{xx}(\mathbf{r}) = J_{xx}(\mathbf{R}_{2J}\mathbf{r}), \quad J_{yy}(\mathbf{r}) = J_{yy}(\mathbf{R}_{2J}\mathbf{r}), \\ &J_{xy}(\mathbf{r}) = J_{xy}(\mathbf{R}_{2J}\mathbf{r}), \quad J_{yx}(\mathbf{r}) = J_{yx}(\mathbf{R}_{2J}\mathbf{r}), \\ &J_{xz}(\mathbf{r}) = -J_{xz}(\mathbf{R}_{2J}\mathbf{r}), \quad J_{yz}(\mathbf{r}) = -J_{yz}(\mathbf{R}_{2J}\mathbf{r}). \end{aligned} \tag{40}$$

Furthermore, the components of the spin-spin correlation meet the relationship

$$\begin{aligned} &J_{xx}(\mathbf{r}) = J_{yy}(\mathbf{R}_{4J}\mathbf{r}), \quad J_{xy}(\mathbf{r}) = -J_{yx}(\mathbf{R}_{4J}\mathbf{r}), \\ &J_{xz}(\mathbf{r}) = J_{yz}(\mathbf{R}_{4J}\mathbf{r}), \quad J_{zx}(\mathbf{r}) = J_{zy}(\mathbf{R}_{4J}\mathbf{r}). \end{aligned} \tag{41}$$

In the x-y plane ($z = 0$), $A_{s\uparrow\uparrow}$ and $A_{s\downarrow\downarrow}$ are real, $A_{s\uparrow\downarrow}(\mathbf{r}) = (-1)^J A_{s\downarrow\uparrow}(\mathbf{r})^*$, and it can be deduced that

$$\begin{aligned} &J_{xy}(\mathbf{r}) = J_{yx}(\mathbf{r}), \quad J_{xz}(\mathbf{r}) = (-1)^J J_{zx}(\mathbf{r}), \\ &J_{yz}(\mathbf{r}) = (-1)^J J_{zy}(\mathbf{r}). \end{aligned} \tag{42}$$

When a magnetic impurity is placed in a multi-Weyl semimetal, the Kondo temperature can be measured to reflect the band properties of the Weyl semimetal. On the other hand, the spin-spin correlation can be used to detect the topological charge of the multi-Weyl semimetals. Experimentally, the spatial anisotropic correlations could be detected in spin-resolved scanning tunneling spectroscope experiments [70–72].

V. CONCLUSION

In conclusion, we investigated spin-1/2 Anderson impurity in a multi-Weyl semimetal. The trial wave-function method was utilized to study the Kondo screening of the impurity at the large Coulomb interaction limit. With the increase in J, a weaker hybridization between the impurity and conduction electrons is required to form a stable bound state. The magnetic impurity and conduction electrons always favor forming a bound state for arbitrary hybridization. The breaking of both time-reversal and inversion symmetries induces an energy difference between two nodal points, and there is no critical value of hybridization Γ_c in this case.

Due to the spin-orbit coupling, the components of spin-spin correlation functions show strong anisotropy in the coordinate

space. The spin-spin correlation indicates distinct decay rates along different directions. The spin-spin correlations for $J = 1$ decay faster along the x axis than in the cases of $J = 2$ and 3. This J-dependent decay behavior of the spin-spin correlations originates from the anisotropic dispersion relationship in the energy band. The topological charge J is reflected in the symmetry of the spin-spin correlations. Most notably, in the cases of $J = 2$ and $J = 3$, there is obvious $\mathbf{C}_{2J}$ symmetry in the spatial spin-spin correlations. Especially, the correlation terms $J_{xx}(x, y, 0)$ and $J_{yy}(x, y, 0)$ and $J_{xy}(x, y, 0)$ and $-J_{yx}(x, y, 0)$ are related to each other by a $\pi/(2J)$ rotation. The rotation symmetry in the spatial spin-spin correlations is expected to be used to probe the winding number in a multi-Weyl semimetal.

ACKNOWLEDGMENTS

This work was supported by the Natural Science Foundation of China under Grants No. 61474018 and No. 11574173, the Fundamental Research Funds for the Central Universities (Grant No. ZYGX2016J064), and the Open Project of the State Key Laboratory of Low-Dimensional Quantum Physics (Grant No. KF201709).

APPENDIX: KONDO TEMPERATURE IN MULTI-WEYL SEMIMETALS

In the presence of diluted magnetic impurities the system is described by the Hamiltonian $H = H_0 + H_J$, and

$$H_J = J_{sd}\sum_{k,k'}(c^\dagger_{k\uparrow}c_{k'\uparrow} - c^\dagger_{k\downarrow}c_{k'\downarrow})S_z + J_{sd}\sum_{k,k'}(c^\dagger_{k\uparrow}c_{k'\downarrow}S^- + c^\dagger_{k\downarrow}c_{k'\uparrow}S^+), \tag{A1}$$

where S is the magnetic moment of the impurities and J_{sd} is the strength of the (antiferromagnetic) coupling between the impurities and the carriers. Here we consider the case of a magnetic impurity with $|S| = 1/2$, and then S can be expressed in terms of auxiliary creation (annihilation) fermionic operators $f^\dagger_\sigma$ (f_σ) satisfying the constraint $n_f = \sum_\sigma f^\dagger_\sigma f_\sigma = 1$. In terms of the f operators, the coupling term H_J can be expressed as

$$H_J = J_{sd}\sum_{k,k';\sigma,\sigma'} c^\dagger_{k\sigma}c_{k'\sigma'}f^\dagger_\sigma f_{\sigma'}. \tag{A2}$$

In the following discussion, the large-N expansion would be performed to make a mean-field treatment of the Kondo problem [58], which was first introduced by Read and Newns [73]. In this method, a Stratonovich-Hubbard transformation is used to eliminate the four-fermion term in favor of a path integral over an auxiliary Bose field $\Delta = \sum_{k,\sigma}\langle c^\dagger_{k\sigma}f_\sigma\rangle$. An integral over a variable is used to enforce the constraint $n_f = 1$ by the introduction of a Lagrange multiplier λ. The fermionic fields then occur only in a quadratic exponent and can be integrated out in closed form, leaving a path integral over Δ and an integral over λ to be evaluated. A $1/N$ expansion can then be obtained from a saddle-point expansion for these integrals. Approximating Δ and λ as static mean fields, the effective action is obtained as [68]

$$S_{\text{eff}} = \frac{1}{k_BT}\left[\frac{2}{\pi}\int d\varepsilon \frac{\arctan\left[\frac{\pi}{2}\frac{\Delta^2\rho(\varepsilon)}{\varepsilon-\mu-\lambda}\right]}{e^{(\varepsilon-\mu)/k_BT}+1} + \frac{\Delta^2}{J_{sd}} - \lambda\right], \tag{A3}$$

where the integral is bound between $-\Lambda$ and Λ, Λ is the cutoff, and $\rho(\varepsilon)$ is the density of states of the Weyl semimetals. By minimizing S_{eff}, we can obtain the self-consistent equations for Δ^2 and λ,

$$\int d\varepsilon \frac{4\rho(\varepsilon)(\varepsilon-\mu-\lambda)/[e^{(\varepsilon-\mu)/k_BT}+1]}{4(\varepsilon-\mu-\lambda)^2+\pi^2\Delta^4\rho^2(\varepsilon)} = -\frac{1}{J_{sd}},$$
$$\int d\varepsilon \frac{4\Delta^2\rho(\varepsilon)/[e^{(\varepsilon-\mu)/k_BT}+1]}{4(\varepsilon-\mu-\lambda)^2+\pi^2\Delta^4\rho^2(\varepsilon)} = 1. \tag{A4}$$

The Kondo temperature T_K can be identified as the highest temperature for which the self-consistent equations have a nontrivial solution.

Here we consider multi-Weyl semimetals with time-reversal symmetry, i.e., $Q = 0$. The retarded Green's function for the free Weyl semimetal has the form

$$G^R_0(\varepsilon, \mathbf{k}) = \frac{1}{\varepsilon+\mu-H_{\mathbf{k}s}+i\delta}, \tag{A5}$$

where $H_{\mathbf{k}s} = s[v_\perp k_0(\tilde{k}^J_-\sigma_+ + \tilde{k}^J_+\sigma_-) + v_zk_z\sigma_z - Q_0]$. The spectral function is then deduced as

$$\begin{aligned}A(\varepsilon,\mathbf{k}) &= -\frac{1}{\pi}\mathrm{Tr}\{\mathrm{Im}[G^R_0(\varepsilon,\mathbf{k})]\}\\ &= 2|\varepsilon+\mu+Q_0|\delta[(\varepsilon+\mu+Q_0)^2-\varepsilon^2_{\mathbf{k}}]\\ &\quad + 2|\varepsilon+\mu-Q_0|\delta[(\varepsilon+\mu-Q_0)^2-\varepsilon^2_{\mathbf{k}}],\end{aligned} \tag{A6}$$

where $\varepsilon_{\mathbf{k}} = v_\perp\sqrt{\frac{k^{2J}_\perp}{k_0^{2J-2}} + \frac{v_z^2}{v_\perp^2}k_z^2}$ and $k^2_\perp = k_x^2 + k_y^2$. The fermion density of states is given by

$$\rho(\varepsilon) = V\int \frac{d^3\mathbf{k}}{(2\pi)^3}A(\varepsilon,\mathbf{k}), \tag{A7}$$

where V is the volume of the system. For the single-Weyl semimetal ($J = 1$), one can obtain [54,68]

$$\rho_s(\varepsilon) = \frac{V}{\pi^2 v_z v_\perp^2}[(\varepsilon+\mu)^2 + Q_0^2]; \tag{A8}$$

for the double-Weyl semimetal ($J = 2$),

$$\rho_d(\varepsilon) = \frac{Vk_0}{8\pi v_z v_\perp}[|\varepsilon+\mu+Q_0| + |\varepsilon+\mu-Q_0|], \tag{A9}$$

and for the triple-Weyl semimetal ($J = 3$),

$$\rho_t(\varepsilon) = \frac{V\Gamma(\frac{1}{3})k_0^{4/3}}{12\pi^{3/2}\Gamma(\frac{5}{6})v_z v_\perp^{2/3}}[|\varepsilon+\mu+Q_0|^{2/3} + |\varepsilon+\mu-Q_0|^{2/3}]. \tag{A10}$$

In the limit of $k_BT \ll \mu \ll \Lambda$ and assuming $Q_0 = 0$ for simplicity, the Kondo temperature T_K for $J = 1$ can be simplified as

$$T_K = \Lambda\exp\left[\frac{1-2/[J_{sd}\rho_s(\Lambda)]}{2\mu^2/\Lambda^2}\right]. \tag{A11}$$

The Anderson Hamiltonian leads us to the degenerate exchange model by performing the Schrieffer-Wolf transformation. The coupling parameters J_{sd} are related to those of the Anderson Hamiltonian, and $J_{sd} = V_{\mathbf{k}}^2/(\varepsilon_d - \mu)$ in the limit $U \to \infty$. The Kondo temperature T_K can also be expressed as [68]

$$T_K = \Lambda \exp\left[\frac{1 - 2\pi^2 v_z v_\perp^2 (\varepsilon_d - \mu)/\left(V_{\mathbf{k}}^2 V \Lambda^2\right)}{2\mu^2/\Lambda^2}\right], \tag{A12}$$

which is consistent with Eq. (21). For $J = 2$, the Kondo temperature T_K can be simplified as

$$T_K = \kappa(\mu) \exp\left[\frac{1 - 1/[J_{sd}\rho_d(\Lambda)]}{|\mu|/\Lambda}\right], \tag{A13}$$

where $\kappa(\mu) = \frac{\mu^2}{\Lambda}$ for $\mu > 0$ and $\kappa(\mu) = \Lambda$ for $\mu < 0$. The Kondo temperature of $J = 2$ is similar to the results of a single-Weyl semimetal in the two-dimensional case Refs. [48] and [68]. In both cases the density of states $\rho(\varepsilon)$ indicates the linear dependence on energy.

[1] B. J. Yang and N. Nagaosa, Nat. Commun. **5**, 4898 (2014).
[2] T. Wehling, A. Black-Schaffer, and A. Balatsky, Adv. Phys. **63**, 1 (2014).
[3] O. Vafek and A. Vishwanath, Annu. Rev. Condens. Matter Phys. **5**, 83 (2014).
[4] M. Yan, H. Huang, K. Zhang, E. Wang, W. Yao, K. Deng, G. Wan, H. Zhang, M. Arita, H. Yang, Z. Sun, H. Yao, Y. Wu, S. Fan, W. Duan, and S. Zhou, Nat. Commun. **8**, 257 (2017).
[5] N. P. Armitage, E. J. Mele, and A. Vishwanath, Rev. Mod. Phys. **90**, 015001 (2018).
[6] M. Lv and S.-C. Zhang, Int. J. Mod. Phys. B **27**, 1350177 (2013).
[7] C.-X. Liu, P. Ye, and X.-L. Qi, Phys. Rev. B **87**, 235306 (2013).
[8] N. Alidoust, S. Y. Xu, I. Belopolski, G. Bian, H. Zheng, D. S. Sanchez, T. Neupert, M. Z. Hasan, Z. Yuan, and C. Zhang, Nat. Phys. **11**, 748 (2015).
[9] A. A. Burkov and L. Balents, Phys. Rev. Lett. **107**, 127205 (2011).
[10] B. Q. Lv, H. M. Weng, B. B. Fu, X. P. Wang, H. Miao, J. Ma, P. Richard, X. C. Huang, L. X. Zhao, G. F. Chen, Z. Fang, X. Dai, T. Qian, and H. Ding, Phys. Rev. X **5**, 031013 (2015).
[11] A. A. Burkov, M. D. Hook, and L. Balents, Phys. Rev. B **84**, 235126 (2011).
[12] X. Wan, A. M. Turner, A. Vishwanath, and S. Y. Savrasov, Phys. Rev. B **83**, 205101 (2011).
[13] S.-Y. Xu, I. Belopolski, N. Alidoust, M. Neupane, G. Bian, C. Zhang, R. Sankar, G. Chang, Z. Yuan, C.-C. Lee, S.-M. Huang, H. Zheng, J. Ma, D. S. Sanchez, B. Wang, A. Bansil, F. Chou, P. P. Shibayev, H. Lin, S. Jia, and M. Z. Hasan, Science **349**, 613 (2015).
[14] C. Fang, Y. Chen, H.-Y. Kee, and L. Fu, Phys. Rev. B **92**, 081201 (2015).
[15] L. M. Schoop, M. N. Ali, C. Straßer, A. Topp, A. Varykhalov, D. Marchenko, V. Duppel, S. S. P. Parkin, B. V. Lotsch, and C. R. Ast, Nat. Commun. **7**, 11696 (2016).
[16] M. Neupane, I. Belopolski, M. M. Hosen, D. S. Sanchez, R. Sankar, M. Szlawska, S.-Y. Xu, K. Dimitri, N. Dhakal, P. Maldonado, P. M. Oppeneer, D. Kaczorowski, F. Chou, M. Z. Hasan, and T. Durakiewicz, Phys. Rev. B **93**, 201104 (2016).
[17] C. Chen, X. Xu, J. Jiang, S.-C. Wu, Y. P. Qi, L. X. Yang, M. X. Wang, Y. Sun, N. B. M. Schröter, H. F. Yang, L. M. Schoop, Y. Y. Lv, J. Zhou, Y. B. Chen, S. H. Yao, M. H. Lu, Y. F. Chen, C. Felser, B. H. Yan, Z. K. Liu, and Y. L. Chen, Phys. Rev. B **95**, 125126 (2017).
[18] R. Singha, A. K. Pariari, B. Satpati, and P. Mandal, Proc. Natl. Acad. Sci. U.S.A. **114**, 2468 (2017).
[19] G. Bian, T.-R. Chang, S. Raman, S.-Y. Xu, H. Zheng, N. Titus, C.-K. Chiu, S.-M. Huang, G. Chang, B. Ilya *et al.*, Nat. Commun. **7**, 10556 (2016).
[20] Y. Wu, L. L. Wang, E. Mun, D. D. Johnson, D. Mou, L. Huang, Y. Lee, S. L. Budko, P. C. Canfield, and A. Kaminski, Nat. Phys. **12**, 667 (2016).
[21] O. Türker and S. Moroz, Phys. Rev. B **97**, 075120 (2018).
[22] W. Wu, Y. Liu, S. Li, C. Zhong, Z.-M. Yu, X.-L. Sheng, Y. X. Zhao, and S. A. Yang, Phys. Rev. B **97**, 115125 (2018).
[23] S. Murakami, New J. Phys. **9**, 356 (2007).
[24] R. Bi, Z. Yan, L. Lu, and Z. Wang, Phys. Rev. B **96**, 201305 (2017).
[25] H. Nielsen and M. Ninomiya, Nucl. Phys. B **185**, 20 (1981).
[26] H. Nielsen and M. Ninomiya, Nucl. Phys. B **193**, 173 (1981).
[27] A. A. Zyuzin, S. Wu, and A. A. Burkov, Phys. Rev. B **85**, 165110 (2012).
[28] Z. Wang and S.-C. Zhang, Phys. Rev. B **87**, 161107 (2013).
[29] H. Wei, S.-P. Chao, and V. Aji, Phys. Rev. Lett. **109**, 196403 (2012).
[30] C. Fang, M. J. Gilbert, X. Dai, and B. A. Bernevig, Phys. Rev. Lett. **108**, 266802 (2012).
[31] G. Xu, H. Weng, Z. Wang, X. Dai, and Z. Fang, Phys. Rev. Lett. **107**, 186806 (2011).
[32] S.-M. Huang, S.-Y. Xu, I. Belopolski, C.-C. Lee, G. Chang, T.-R. Chang, B. Wang, N. Alidoust, G. Bian, M. Neupane, D. Sanchez, H. Zheng, H.-T. Jeng, A. Bansil, T. Neupert, H. Lin, and M. Z. Hasan, Proc. Natl. Acad. Sci. U.S.A. **113**, 1180 (2016).
[33] Q. Liu and A. Zunger, Phys. Rev. X **7**, 021019 (2017).
[34] G. E. Volovik, *The Universe in a Helium Droplet* (Clarendon, Oxford, 2003).
[35] P. Goswami and L. Balicas, arXiv:1312.3632 (2013).
[36] P. Goswami and A. H. Nevidomskyy, Phys. Rev. B **92**, 214504 (2015).
[37] M. H. Fischer, T. Neupert, C. Platt, A. P. Schnyder, W. Hanke, J. Goryo, R. Thomale, and M. Sigrist, Phys. Rev. B **89**, 020509 (2014).
[38] B. Roy, S. A. A. Ghorashi, M. S. Foster, and A. H. Nevidomskyy, Phys. Rev. B **99**, 054505 (2019).
[39] R. M. A. Dantas, F. Peña-Benitez, B. Roy, and P. Surówka, J. High Energy Phys. 12 (2018) 069.
[40] S. Ahn, E. J. Mele, and H. Min, Phys. Rev. B **95**, 161112 (2017).
[41] S. Park, S. Woo, E. J. Mele, and H. Min, Phys. Rev. B **95**, 161113 (2017).

[42] T. Hayata, Y. Kikuchi, and Y. Tanizaki, Phys. Rev. B **96**, 085112 (2017).
[43] Z.-M. Huang, J. Zhou, and S.-Q. Shen, Phys. Rev. B **96**, 085201 (2017).
[44] Y. Sun and A. Wang, J. Phys.: Condens. Matter **29**, 435306 (2017).
[45] B. Roy, P. Goswami, and V. Juričić, Phys. Rev. B **95**, 201102 (2017).
[46] P. W. Anderson, Phys. Rev. **124**, 41 (1961).
[47] A. V. Balatsky, I. Vekhter, and J.-X. Zhu, Rev. Mod. Phys. **78**, 373 (2006).
[48] X.-Y. Feng, W.-Q. Chen, J.-H. Gao, Q.-H. Wang, and F.-C. Zhang, Phys. Rev. B **81**, 235411 (2010).
[49] H.-F. Lü, H.-Z. Lu, S.-Q. Shen, and T.-K. Ng, Phys. Rev. B **87**, 195122 (2013).
[50] B. Uchoa, V. N. Kotov, N. M. R. Peres, and A. H. Castro Neto, Phys. Rev. Lett. **101**, 026805 (2008).
[51] M. Killi, D. Heidarian, and A. Paramekanti, New J. Phys. **13**, 053043 (2011).
[52] X. Lin and J. Ni, Phys. Rev. B **86**, 075440 (2012).
[53] S.-C. Lu and J.-P. Leburton, Nanoscale Res. Lett. **9**, 676 (2014).
[54] A. K. Mitchell and L. Fritz, Phys. Rev. B **92**, 121109 (2015).
[55] J.-H. Sun, D.-H. Xu, F.-C. Zhang, and Y. Zhou, Phys. Rev. B **92**, 195124 (2015).
[56] J.-H. Sun, L.-J. Wang, X.-T. Hu, L. Li, and D.-H. Xu, Phys. Rev. B **97**, 035130 (2018).
[57] C. Kittel, *Quantum Theory of Solids* (Wiley, New York, 1963).
[58] A. Hewson, *The Kondo Problem to Heavy Fermions* (Cambridge University Press, Cambridge, 1997).
[59] H. R. Chang, J. Zhou, S. X. Wang, W. Y. Shan, and D. Xiao, Phys. Rev. B **92**, 241103 (2015).
[60] M. V. Hosseini and M. Askari, Phys. Rev. B **92**, 224435 (2015).
[61] D. Mastrogiuseppe, N. Sandler, and S. E. Ulloa, Phys. Rev. B **93**, 094433 (2016).
[62] S. P. Mukherjee and J. P. Carbotte, Phys. Rev. B **97**, 045150 (2018).
[63] H. G. Luo, T. Xiang, X. Q. Wang, Z. B. Su, and L. Yu, Phys. Rev. Lett. **92**, 256602 (2004).
[64] J. D. Lee, Phys. Rev. B **61**, 8062 (2000).
[65] Z. Wang, Y. Sun, X.-Q. Chen, C. Franchini, G. Xu, H. Weng, X. Dai, and Z. Fang, Phys. Rev. B **85**, 195320 (2012).
[66] Z. K. Liu, L. X. Yang, Y. Sun, T. Zhang, H. Peng, H. F. Yang, C. Chen, Y. Zhang, Y. F. Guo, D. Prabhakaran, M. Schmidt, Z. Hussain, S. K. Mo, C. Felser, B. Yan, and Y. L. Chen, Nat. Mater. **15**, 27 (2015).
[67] C. M. Varma and Y. Yafet, Phys. Rev. B **13**, 2950 (1976).
[68] A. Principi, G. Vignale, and E. Rossi, Phys. Rev. B **92**, 041107 (2015).
[69] D. Ma, H. Chen, H. Liu, and X. C. Xie, Phys. Rev. B **97**, 045148 (2018).
[70] V. Madhavan, W. Chen, T. Jamneala, M. F. Crommie, and N. S. Wingreen, Science **280**, 567 (1998).
[71] M. R. Calvo, J. Fernández-Rossier, J. J. Palacios, D. Jacob, D. Natelson, and C. Untiedt, Nature (London) **458**, 1150 (2009).
[72] H. D. Chopra, M. R. Sullivan, J. N. Armstrong, and S. Z. Hua, Nat. Mater. **4**, 832 (2005).
[73] N. Read and D. M. Newns, J. Phys. C: Solid State Phys. **16**, 3273 (1983).